TORNADOES in HURRICANE HARVEY:
DOCUMENTATION and ENVIRONMENTAL ANALYSIS

Roger Edwards[1]
NWS Storm Prediction Center, Norman, OK

Christopher J. Nowotarski
Texas A&M University, College Station, TX

Scott Overpeck
NWS Forecast Office, League City, TX

Gary R. Woodall
NWS Forecast Office, Memphis, TN

1. BACKGROUND

a. General concepts

Tropical cyclones (TCs) offer a variety of hazards during their landfall phases, including their own damaging gradient winds and gusts, storm surge, inland flooding from heavy rainfall, and tornadoes. The risks from flooding and tornadoes, in particular, often shift inland great distances during the days after landfall, their duration depending both on translation of the TC and favorable atmospheric conditions within the remnants. The threat of tornadoes from TCs has been documented and analyzed in climatological and statistical terms for almost a century (e.g., Barbour 1924; Hill et al. 1966; Novlan and Gray 1974; McCaul 1991; Verbout et al. 2007; Edwards 2012, hereafter E12; Moore et al. 2017; among numerous others).

Forecasting TC tornado scenarios has evolved from a climatologically based exercise to one involving physical concepts responsible for their distributions, which are typically in the middle to outer sector of the circulation, from roughly north through south-southeast of center (E12 and related references). In subtropical and middle latitudes of U.S. landfalls, that sector normally is downshear with respect to measures of deep-tropospheric shear (e.g., the 850–200-hPa layer operationally used in TC forecasting, following Kaplan and DeMaria 2003). The same sector typically contains the most favorable juxtapositions of the same four environmental ingredients sought for predicting midlatitude supercellular tornadoes, from an ingredients-based framework (e.g., Johns and Doswell 1992, as applied to severe-storms forecasting):

- Moisture: rarely deficient in TCs.
- Instability: usually marginal, yet also highly variable in TCs, often a strong operational forecasting uncertainty on >6-h time scales of Storm Prediction Center (SPC) outlooks. With

lapse rates above the boundary layer often near moist adiabatic, small differences in boundary-layer diabatic heating and lapse rates, related to meso-β and smaller-scale cloud-cover and precipitation areas, either can introduce CAPE quickly where none existed, or modulate CAPE by orders of magnitude from ~10^0 to ~10^3 J kg^{-1}.

- Lift (convective scale): spiral bands, frontal zones, outflow boundaries, differential-heating boundaries, and convergence lines, either pre-existing in the TC or encountered by it. Edwards and Pietrycha (2006) show archetypes for the influence of such embedded boundaries on near-term, mesoscale tornado potential.
- Vertical wind shear: examined mainly in the lower troposphere for TC tornado-forecasting purposes, due to the relatively shallow nature of tornadic TC supercells. Low-level shear vectors and hodograph sizes typically are larger than those for tornadic midlatitude supercells, given the relatively intense flow in the middle-upper boundary layer.

While TCs fall under the National Hurricane Center's (NHC's) forecast responsibility, SPC coordinates tornado-threat verbiage in NHC's advisories, and issues outlooks, mesoscale discussions and watches for the CONUS tornado threat. Local NWS offices issue tornado warnings and follow-up severe-weather statements. See Edwards et al. (2015a) for more details on the SPC forecast suite; examples of SPC products specific to Hurricane Harvey of 2017 are provided in section 4.

The WSR-88D-era dataset of TC tornadoes (TCTOR; Edwards 2010), developed and maintained at the SPC, contains 1435 records from 1995–2017. This represents 5% of the national tornado total for the same period in the "ONETOR" (Schaefer and Edwards 1999) database. Tornadoes accounted for 3% of TC-related fatalities from 1963–2012 (Rappaport 2014). TC tornadoes pose a challenge

---
[1] *Corresponding author address:* Roger Edwards, Storm Prediction Center, National Weather Center, 120 Boren Blvd #2300, Norman, OK 73072; E-mail: roger.edwards@noaa.gov

for warning purposes since they tend to be smaller, shorter-lived, and more difficult to spot than their midlatitude supercellular counterparts (E12), and to occur in supercells that are more compressed in the horizontal and vertical, as well as messier in mode, with weaker radar rotational velocities and smaller mesocyclones (e.g., Spratt et al. 1997; E12; Edwards et al. 2012; Edwards et al. 2015b).

TC tornadoes also can be more difficult to document and verify, given that their typically weak, EF0–EF1 damage on the Enhanced Fujita Scale (Edwards et al. 2013) may be masked by TC wind and hydraulic effects near the coast, and/or occur in remote areas with few damage indicators. The dual-polarization WSR-88D upgrades this decade have enabled more efficient and reliable tornado indication, in particular via the presence of debris in cross-correlation coefficient fields as the tornadic detection signature (TDS; Rhyzhkov et al. 2005). The TDS has improved tornadic verification and survey-targeting capabilities, especially in remote areas and TC settings, where the signature is often quite well-defined amidst nearly homogeneous warm-rain returns (Edwards and Picca 2016).

b. Hurricane Harvey

Blake and Zelinsky (2018) provide the full National Hurricane Center (NHC) report on Harvey, including track, intensity, NHC forecasts and verification, and overview of impacts. In summary, Harvey began as a tropical wave moving off West Africa on 12 August 2017, very slowly and unevenly organizing across the tropical Atlantic, before becoming a depression on 17 August, east of Barbados. After briefly strengthening into a marginal tropical storm, Harvey devolved back to an open wave over the central Caribbean on 19 August. In the remnant trough, a closed low formed again over the Yucatan Peninsula of Mexico on 22 August, intensifying to a tropical depression the next day over the Bay of Campeche.

The newly re-formed cyclone rapidly intensified as it moved northward over warm water of the western Gulf of Mexico, amidst weak tropospheric shear. Harvey became a major (category 3) hurricane by midday local time 25 August, offshore from the lower–middle Texas coast, on the first of its seven local calendar days of tornado production (section 2). By 00 UTC 26 August, 3 h before initial landfall near Rockport, TX, Harvey became a category 4 hurricane with estimated sustained winds of 115 kt (59 m s^{-1}), and minimum central MSL pressure of 937 hPa.

Following initial landfall (Fig. 1), Harvey's center moved inland and decelerated amidst weak ambient steering flow, performing a slow translational path loop over the middle Texas coastal plain on 26–27 August. Meanwhile, it maintained tropical storm intensity with a substantial fraction of the circulation envelope still over the Gulf. The center moved back offshore around 0300 UTC 28 August near Matagorda Bay, TX, crossed the Gulf south of Galveston, TX, and moved ashore again near Cameron, LA, at 0800 UTC 30 August, all with maximum sustained winds in the lowest 10 kt (5 m s^{-1}) of tropical storm strength. NHC downgraded Harvey to a tropical depression late

on 30 August, and to an extratropical cyclone by 0600 UTC 1 September, slightly over an hour after the final confirmed tornado over middle Tennessee.
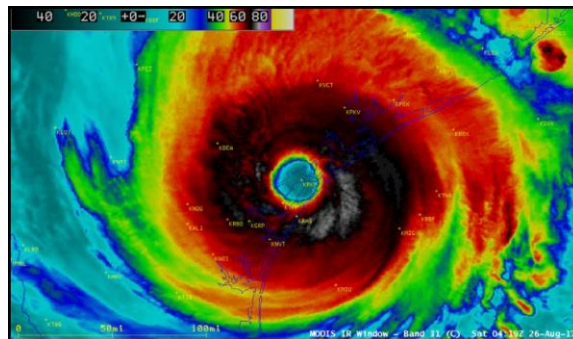

Figure 1: Enhanced infrared satellite image of Harvey near initial landfall, with Rockport, TX in the eye, 0419 UTC 26 August 2017. From the NASA moderate-resolution imaging spectroradiometer (MODIS), via Blake and Zelinsky (2018).

The primary hazard and impact from Harvey was flooding related to extremely heavy rain of long duration. During its multi-day presence over the middle–upper Texas coastal plain, Harvey produced record rainfall amounts for a U.S. TC. A gauge near Nederland, TX, measured a peak storm total of 60.58 in (1539 mm) at Nederland, TX, with 36–48 in (914–1219 mm) over the Houston metro area, and numerous amounts >40 in (1016 mm) from south and east of Houston to near Lake Charles, LA. NSSL Multi-Radar, Multi-Sensor quantitative precipitation-estimation algorithms (Zhang 2015) yielded potential totals approaching 70 in (1778 mm) in remote, rural areas of the southeast Texas coastal plain that lacked in situ gauges. As a result, the Houston and Beaumont/Port Arthur, TX, metro areas experienced catastrophic, unprecedented flooding, with ≈300 000 structures and ≈500 000 cars inundated.

Tornadoes were a far lesser hazard than heavy rain, in terms of impacting life and property, but still justify analysis, given their large number (52 total) and unprecedented cumulative threat duration. The tornadic setting of Harvey during its meandering, weeklong tornadic phase is examined in this work, with section 2 documenting and mapping the tornadoes, section 3 summarizing meteorological characteristics, and section 4 on SPC forecasts. Section 5 offers concluding remarks, discussion and potential avenues for additional research.

2. TORNADO CHARACTERISTICS

a. Overview and outstanding events

Harvey spawned 52 known tornadoes in a weeklong cumulative episode: seven local calendar days and eight UTC days. By either time delineation, this represents a record number of *consecutive* tornado days for one U.S. TC, not only in the TCTOR era but the entire prior U.S. tornado record (per the quality-controlled ONETOR version analyzed in Verbout et al. 2007). Figure 2 puts Harvey's tornado count in the context of 2017 and TCTOR as a whole across years,
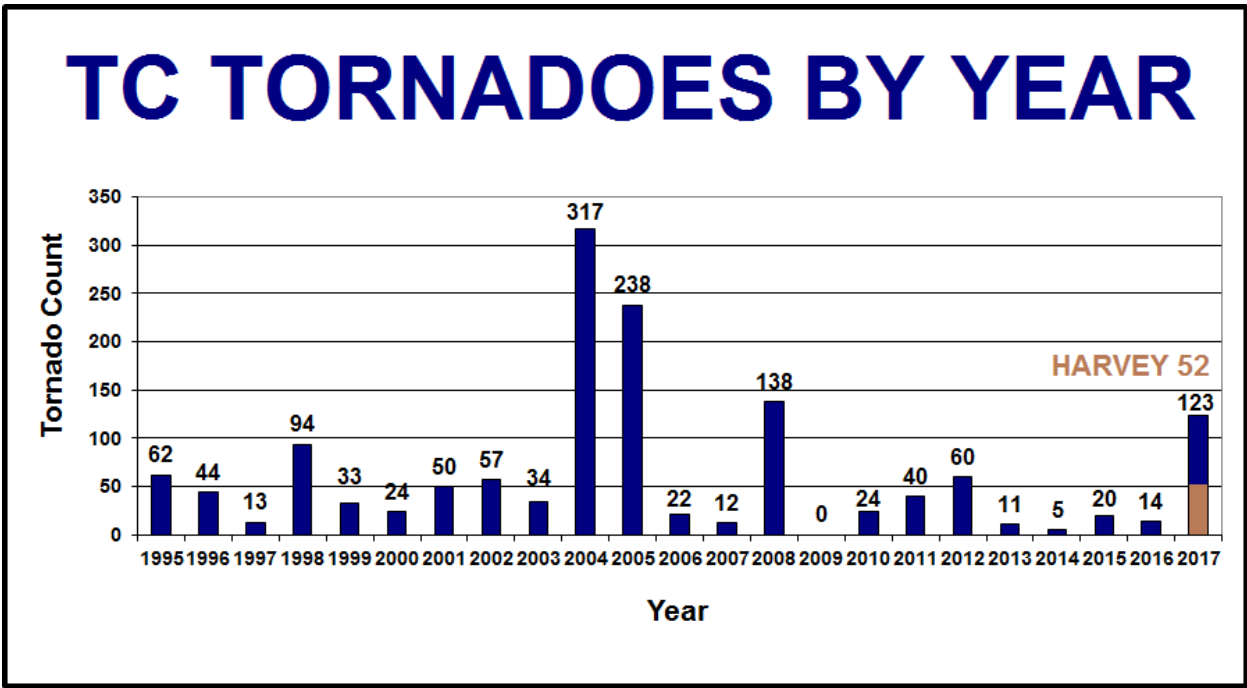
Figure 2: Bar chart of tornado counts from the 1995–2017 SPC TCTOR dataset, with Harvey's contribution in tan.

Table 1: Harvey (tan shading) ranked among the top 10 U.S. tornado-producing TCs on record, using NHC mainland U.S. landfall classification of hurricane (H) or tropical storm (TS).

TROPICAL CYCLONE	YEAR	TORNADO REPORTS
H Ivan	2004	118
H Beulah	1967	115
H Frances	2004	103
H Rita	2005	98
H Katrina	2005	59
H Andrew	1992	56
H Harvey	2017	52
TS Fay, H Gustav	2008	49
H Georges, TS Cindy	1998, 2005	48

3

Table 2: Chronological listing of tornadoes in Harvey, 25 August to 1 September 2017 (UTC). Subtract 5 h for local time (CDT). Time, county (or parish for LA), latitude, and longitude are for tornadogenesis. Ratings use peak EF-scale damage. Path length is in km, (max) path width in m. Destruction potential index (DPI) is unitless, per Thompson and Vescio (1998). No tornado fatalities were recorded; INJ stands for injuries.

#	DATE	TIME	STATE	COUNTY	LAT.	LON.	EF	INJ.	LENGTH	WIDTH	DPI
1	25	1918	TX	Galveston	29.31	-94.77	0	0	0.2	18	0.001
2	25	2030	TX	Brazoria	28.98	-95.48	0	0	0.4	27	0.004
3	25	2108	TX	Matagorda	28.77	-95.63	1	0	3.5	46	0.124
4	25	2114	TX	Calhoun	28.42	-96.67	0	0	0.3	18	0.002
5	25	2311	TX	Brazoria	29.15	-95.54	0	0	6.4	46	0.113
6	26	344	TX	Brazoria	29.22	-95.35	0	0	7.7	46	0.135
7	26	528	TX	Brazoria	29.3	-95.3	0	0	6.9	46	0.122
8	26	550	TX	Brazoria	29.44	-95.45	0	0	2.5	46	0.045
9	26	556	TX	Fort Bend	29.49	-95.52	1	0	2.4	91	0.166
10	26	710	TX	Wharton	29.34	-96.25	0	0	2.3	27	0.025
11	26	712	TX	Fort Bend	29.7	-95.76	0	0	0.2	27	0.002
12	26	930	TX	Harris	29.92	-95.15	0	0	1.6	27	0.017
13	26	1000	TX	Fort Bend	29.78	-95.84	1	0	0.6	46	0.023
14	26	1305	TX	Brazos	30.48	-96.31	0	0	0.3	18	0.002
15	26	1722	LA	Cameron	29.97	-93.35	0	0	2.7	23	0.024
16	26	2050	TX	Harris	29.91	-95.69	1	0	1.5	46	0.053
17	26	2120	TX	Harris	29.95	-95.67	0	0	0.8	46	0.015
18	26	2223	TX	Wharton	29.54	-96.08	0	0	0.9	27	0.009
19	27	115	TX	Fort Bend	29.57	-95.51	1	0	9.3	91	0.657
20	27	500	TX	Harris	29.55	-95.11	0	0	0.05	27	0.001
21	27	643	TX	Wharton	29.52	-96.07	1	0	3.7	46	0.129
22	27	903	TX	Galveston	29.51	-95.01	0	0	1.2	27	0.012
23	27	1515	TX	Harris	29.72	-95.42	0	0	0.1	18	0.001
24	27	1915	LA	Vermilion	29.99	-92.04	0	0	0.3	23	0.003
25	27	1935	LA	Iberia	29.97	-91.76	0	0	0.2	23	0.002
26	28	939	LA	Cameron	29.76	-93.71	0	0	0.5	23	0.004
27	29	2200	LA	Vermilion	29.96	-92.41	0	0	0.03	23	0.0003
28	29	2209	LA	Acadia	30.23	-92.58	2	0	3.5	160	0.65
29	29	2234	LA	Lafayette	30.16	-92.18	0	0	0.2	23	0.002
30	30	600	MS	Harrison	30.4	-88.91	0	0	0.2	27	0.003
31	30	720	MS	Jackson	30.34	-88.55	0	0	0.4	183	0.028
32	30	1504	MS	Lamar	31.16	-89.54	1	0	2.8	91	0.194
33	30	1507	MS	Pearl River	30.72	-89.36	1	0	5.2	183	0.739
34	30	1631	MS	Jackson	30.36	-88.77	0	0	3.7	229	0.33
35	30	1641	MS	Forrest	31.35	-89.27	1	0	2	146	0.229
36	30	1735	MS	Jeff. Davis	31.57	-89.75	0	0	1.7	46	0.031
37	31	1319	AR	Phillips	34.48	-90.62	0	0	2.8	46	0.049
38	31	1657	MS	Benton	34.95	-89.3	0	0	0.4	27	0.005
39	31	1813	MS	Lee	34.31	-88.73	0	0	1.7	37	0.024
40	31	1823	MS	Itawamba	34.43	-88.51	1	0	4	137	0.421
41	31	1843	MS	Prentiss	34.6	-88.57	0	0	0.4	27	0.004
42	31	2007	TN	Hardin	35.23	-88.34	0	0	2	46	0.036

#	DATE	TIME	STATE	COUNTY	LAT.	LON.	EF	INJ.	LENGTH	WIDTH	DPI
43	31	2040	AL	Pickens	33.38	-88.03	2	6	50.3	548	31.95
44	31	2119	TN	Perry	35.54	-87.73	0	0	0.4	46	0.007
45	31	2203	TN	Hardin	35.27	-88.03	0	0	1.2	64	0.03
46	31	2211	TN	Maury	35.52	-87.23	0	0	5.5	69	0.146
47	31	2357	AL	Bibb	32.92	-87.33	1	0	10.5	91	0.739
48	1	28	AL	Bibb	33.1	-87.17	1	0	0.9	183	0.127
49	1	42	AL	Bibb	33.2	-87.13	0	0	0.5	32	0.006
50	1	158	AL	Cullman	34.15	-86.61	2	0	21.9	274	6.97
51	1	421	TN	Davidson	36.21	-86.85	1	0	1	69	0.053
52	1	447	TN	Davidson	36.16	-86.71	0	0	1.5	46	0.027
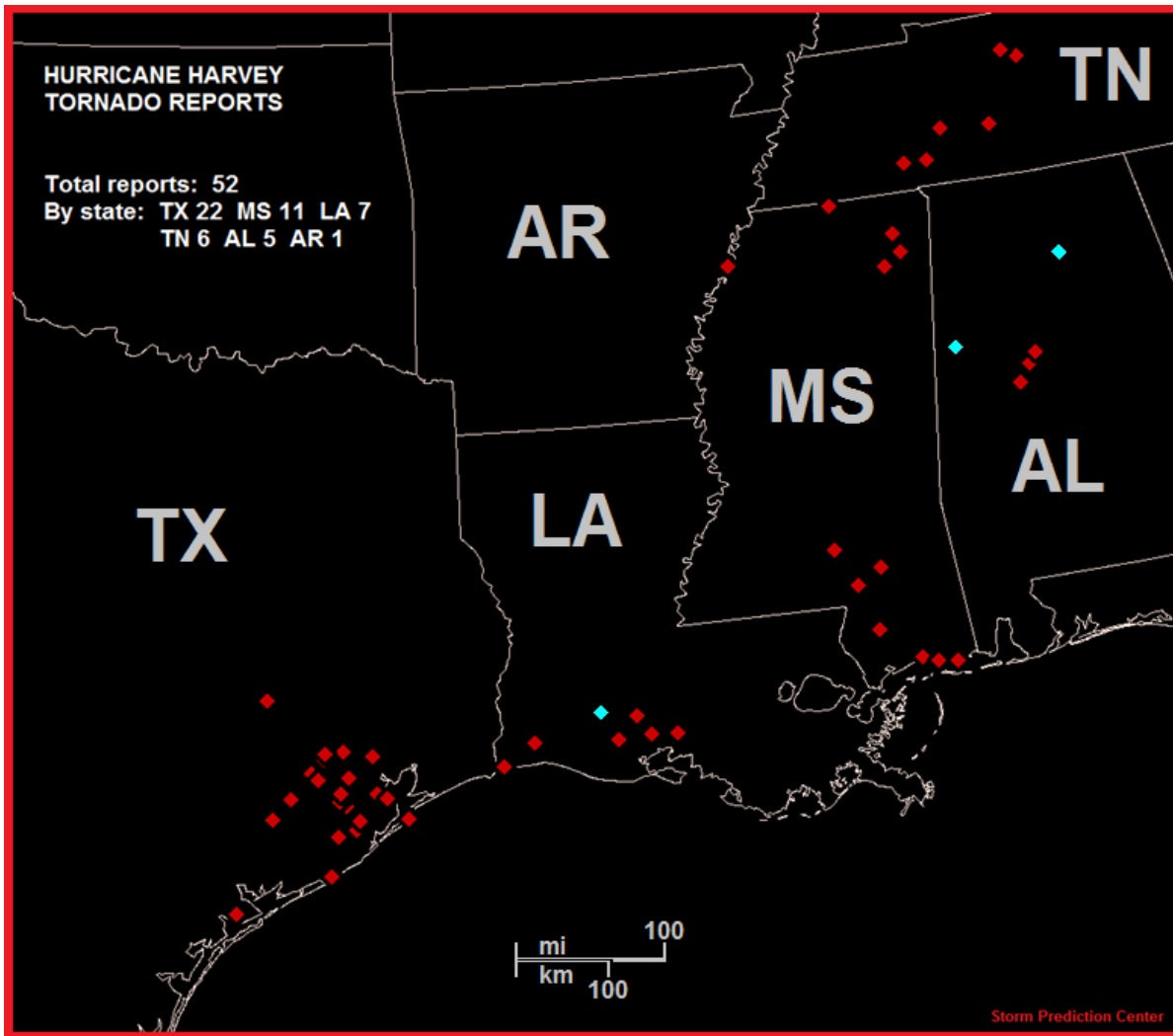
Figure 3: Geographic distribution of tornadoes from Table 2 (red diamonds for EF0 and EF1, cyan for EF2), with state totals in the legend. Some symbols overlap on this scale.

Table 1 ranks Harvey amongst other TCs in the modern record (since 1950), Table 2 lists some characteristics of all of Harvey's tornadoes, and Fig. 3 maps them.

Harvey's tornado tally alone was more than 15 of the prior TC seasons since 1995, and accounted for 42% of the relatively active 2017 TC-tornado season. Tornadoes the first three days were most concentrated over southeast Texas, all of which were classified on the weak (EF0–EF1) portion of the damage spectrum. Damage assessment was limited

logistically by local NWS staffing concerns and often difficulty of access, amidst the widespread, record flooding. Tornadoes hit some of the same counties on different days, including parts of the Houston-Galveston metro area (Brazoria, Harris, Fort Bend, and Galveston County events in Table 2). As the tornadic northeastern sector of Harvey lingered over the area, and flooding worsened, safety messaging in tornado warnings became troublesome, as standard advice to shelter in the lowest levels of homes was both impractical and unsafe in those that were inundated. A relative lull in activity characterized the middle two days of Harvey's tornadic period, with only four reports across southern Louisiana on the 28th and 29th (UTC). Still, one strong (EF2) event was recorded in Acadia Parish (#28 in Table 2).

The largest tornadic path lengths, path widths, areas, and most intense damage (including all EF2s) occurred in the final three days of Harvey's tornadic production from Louisiana across Mississippi to Alabama and Tennessee, and generally farther inland than its southeast Texas phase. This conforms well to general TCTOR characteristics for larger, more damaging TC tornadoes in later, inland TC stages, as analyzed by Moore et al. (2017).

Included in the latter inland phase was the longest-lived, largest, most damaging tornado (#43 in Table 2), and the only one with casualties (6 injuries), beginning at Reform, AL, on the afternoon of 31 August. There, the tornado produced EF2 residential damage, before traveling north-northeastward across eastern Pickens, extreme southeastern Lamar, and western Fayette Counties with up to EF1 tree damage. This tornado yielded more than 2.5 times the Destruction Potential Index (DPI; Thompson and Vescio 1998) of all the other tornadoes in Harvey combined, and had the greatest DPI of any of the 1435 tornadoes in the 1995–2017 TCTOR dataset.

Video and photos of the Reform tornado (e.g., Fig. 4) revealed a sharply defined condensation funnel at times, with intense upward helical motion, occasional multiple-vortex structure, and substantial visual separation of the heavy-precipitation core from the tornado. In contrast to the messy, rain-wrapped modes of many TC supercells (Edwards et al. 2012), the Reform event exhibited visual and radar characteristics (Fig. 5) resembling that of classic, nontropical tornadic supercells in the Great Plains and Midwest. Such storm structure and tornado behavior has been observed with other tornadic supercells in inland TC-decay stages well after landfall, including Danny of 1985, also in northern Alabama (Fig. 10 in McCaul 1987). The Reform tornado resulted in a prominent "debris ball" (Burgess et al. 2002) radar reflectivity signature (Fig. 5 top panel) collocated with a spectrum-width maximum and evidence of a TDS (not shown). Observed rotational velocities of about 60 kt (31 m s^{-1}) fall into the upper quartile of F/EF2 right-moving, supercellular tornado distributions for its radar-distance range, and in the lower-middle quartile for F/EF3 (Smith et al. 2015). This was the final day of Harvey's tornado production, which stopped during the evening of 31 August local time (1 September in UTC) over middle Tennessee, near Nashville.

Figure 4: Frame capture of tornado video near Reform, AL, at about 2050 UTC 31 August 2017.
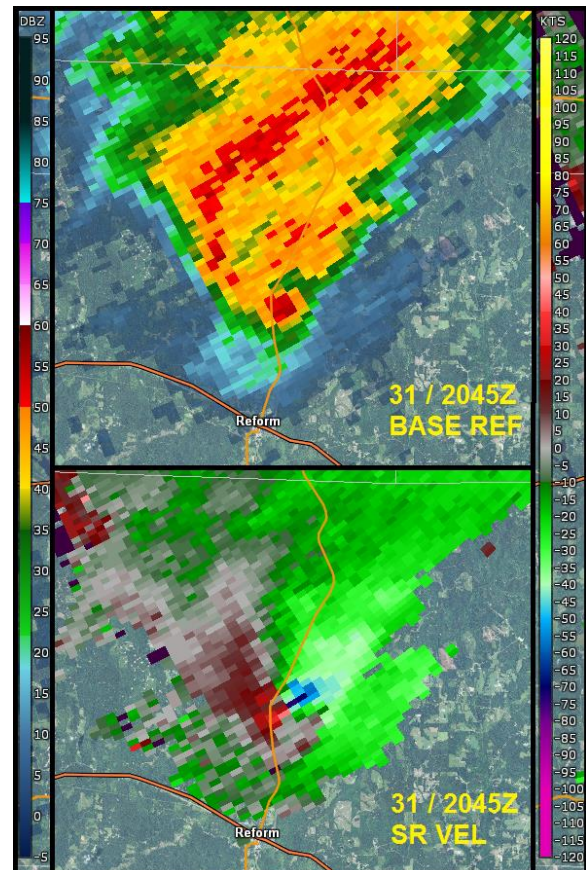

Figure 5: 0.5° base reflectivity (top, scale at left) and storm-relative velocity (bottom, scale at right) presentations of the Reform, AL tornadic supercell from the Columbus Air Force Base, MS, WSR-88D. Base imagery via GRLevel2® software.

b. Climatological comparisons within TCTOR

In the TCTOR era, 1995–2017, only four other TCs produced more tornadoes than Harvey (Table 1), all in the historically active 2004 and 2005 seasons. In terms of total tornadic-phase temporal duration, Tropical Storm Fay was greater, with 8 calendar days and 9 UTC days between 18–28 August 2008; however, Fay had a 2-day tornado-free gap on 21 and 22 August, after the first 2 tornadic days. Harvey yielded more *consecutive* days (7) of tornadoes. When broken down by time of day (Fig. 6), Harvey had a higher proportion of nighttime (≈0000–1159 UTC) tornadoes than TCTOR as a whole. Still, Harvey produced more "daytime" (≈1800-2359 UTC) tornadoes (32, or 61.5%) compared to 20 (38.5%) at "nighttime"[2]. TCTOR at large yields 70.7% and 29.3% of day and night events, respectively.
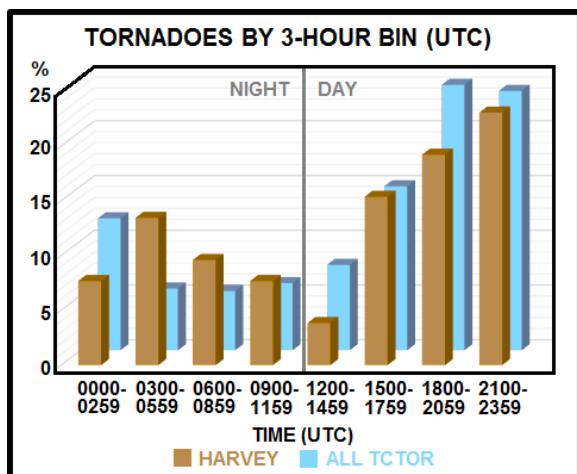
Figure 6: Juxtaposed histograms of percentage of tornadoes in Harvey (front, tan) and 1995–2017 TCTOR (rear, blue), by 3-h time bins in UTC, corresponding approximately to local nocturnal (left) and diurnal (right) 12-hourly categories. All tornadoes occurred within the CDT zone; subtract 5 h from UTC for local time.

The distribution of Harvey's tornado-path characteristics was similar to that of the TC-tornado climatology at large (Fig. 7a–c), except that they were in the lower-middle quartile of the TCTOR radial-distance distribution, and packed somewhat closer to the TC circulation center (Figs. 7d, 8), with similar azimuthal distribution (Fig. 8). The upper part of path length, width and DPI distributions were also somewhat lower in Harvey than those for TCTOR, but with considerable interquartile overlap.

In terms of the damage-rating component of DPI, 37 (71%) of Harvey's tornadoes were rated EF0, 12 (23%) EF1 and 3 (6%) EF2. Harvey's tornadoes were weighted slightly more toward the weakest end

than those of TCTOR as a whole, which shows 64% EF0, 30% EF1 and 6% EF2+, for 1435 events from 1995−2017. However, when binned more coarsely by "weak" and "strong" categories (e.g., Hales 1988) and rounded to whole percentages, Harvey's tornadoes matched those of TCTOR.

3. ENVIRONMENTAL OVERVIEW

Harvey's tornadic-phase meteorological environment is summarized herein from "top down" and the synoptic scale to the mesoscale, with greatest emphasis on the latter, in keeping with the Snellman (1982) "forecast funnel" concept. To start, mandatory-level upper-air charts (not shown) were hand-analyzed for 0000 UTC preceding and during each tornadic day, and 1200 UTC objectively analyzed charts were examined to establish intermediate continuity.

In upper levels (as represented by 250 hPa), synoptic-scale charts showed an anticyclone over Harvey on 25 August moving eastward across the Gulf and away from Harvey on the 26th, becoming elongated southwest–northeast over the Gulf on the 28th, before moving across Florida and over the Atlantic. This occurred conterminously with Harvey's inland penetration and weakening, while a weak trough lingered quasistationary over central and south Texas through the 31st. The 250-hPa winds were westerly to southwesterly across Harvey for much of this period, contributing to the deep shear discussed below. Harvey became entrained into stronger, difluent, southwesterly upper-level flow east of the trough on 29–31 August as the trough assumed negative tilt. At 500 hPa, the circulation of Harvey remained secluded from the midlatitude westerlies until around 29 August at 0000 UTC, when it loosely and briefly phased with a trough extending southwestward from a cold-core low crossing the upper Great Lakes. The intervening height weakness remained largely in place across the Ohio and lower Mississippi Valleys as Harvey gradually turned northeastward.

Midlevel drying, and specifically gradients in 500–700-hPa relative humidity (RH), have been associated with increased tornado production in TCs (Curtis 2004). A 500-hPa dry slot and RH gradient were evident in the outer southern and eastern fringes of Harvey's envelope at 00 UTC 28 August, between Brownsville, TX, and Lake Charles, LA, becoming more pronounced on the 29th and continuing through 1 September. To the extent the balloon-based upper-air data can resolve, the gradient appeared to be located just east of the tornadoes until the second peak of production over the lower Mississippi Valley and Mid-South regions. A 700-hPa dry slot and RH gradient did not juxtapose with the tornadic sector of Harvey until the 31st and 1st; no drying at this level appeared near the Texas and southwestern Louisiana tornadoes.

On the synoptic to meso-*α* scale, ambient deep-layer vertical shear, as an influence of TC interaction with midlatitude westerlies, has been associated not

---

[2] Earlier preliminary analyses of Harvey's tornado times indicated a preference for local morning tornado production. However, systematic time-conversion errors in the initial draft of 2017 national ONETOR were discovered and corrected, subsequently changing Harvey's results to these.
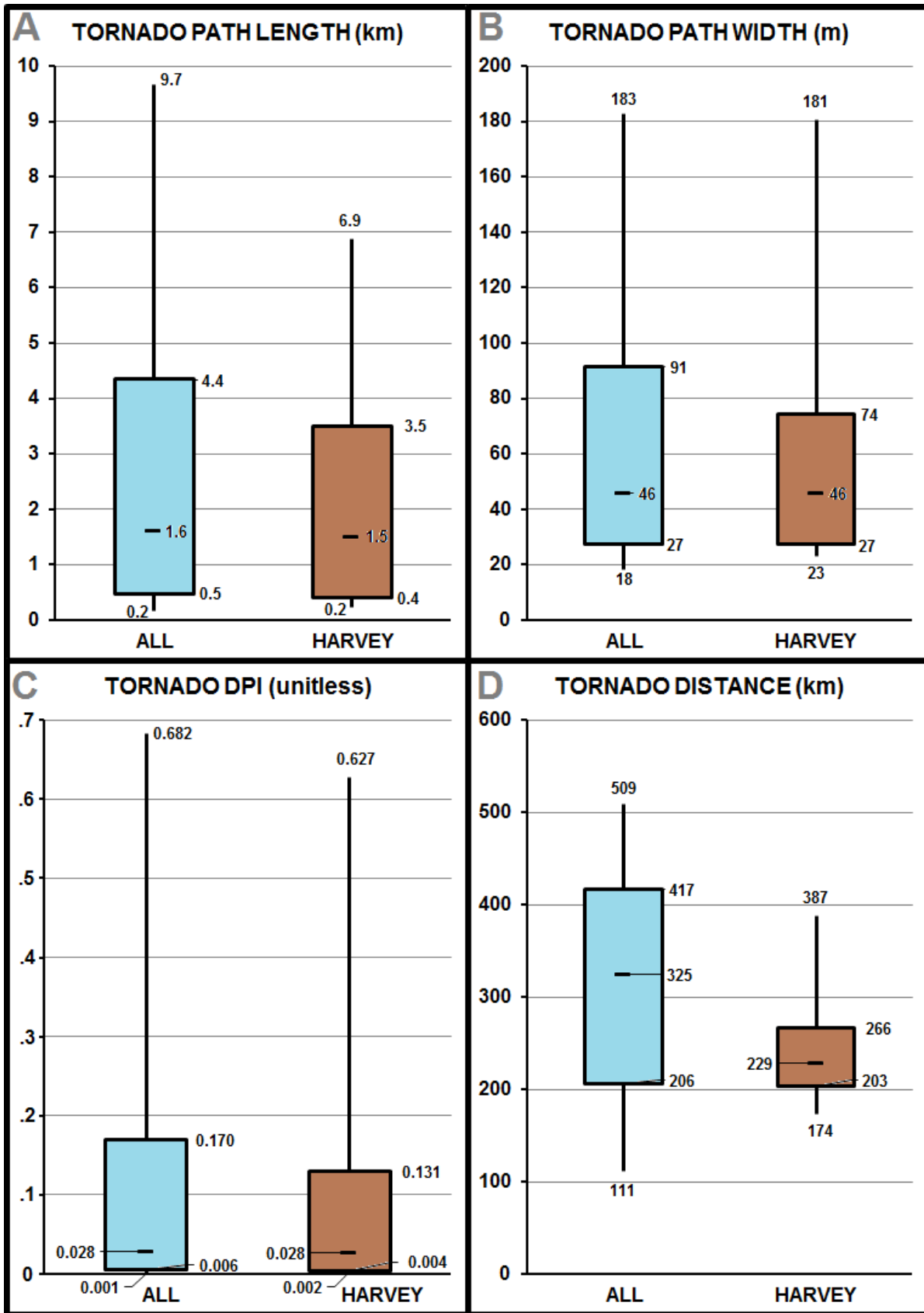
Figure 7: Box plots of 1995–2017 TCTOR path characteristics (light blue) compared to those for Harvey (tan): a) path length, b) path width, c) DPI, and d) distance of tornadogenesis from TC center. Boxes represent middle quartiles; whiskers extend to 90th percentiles.
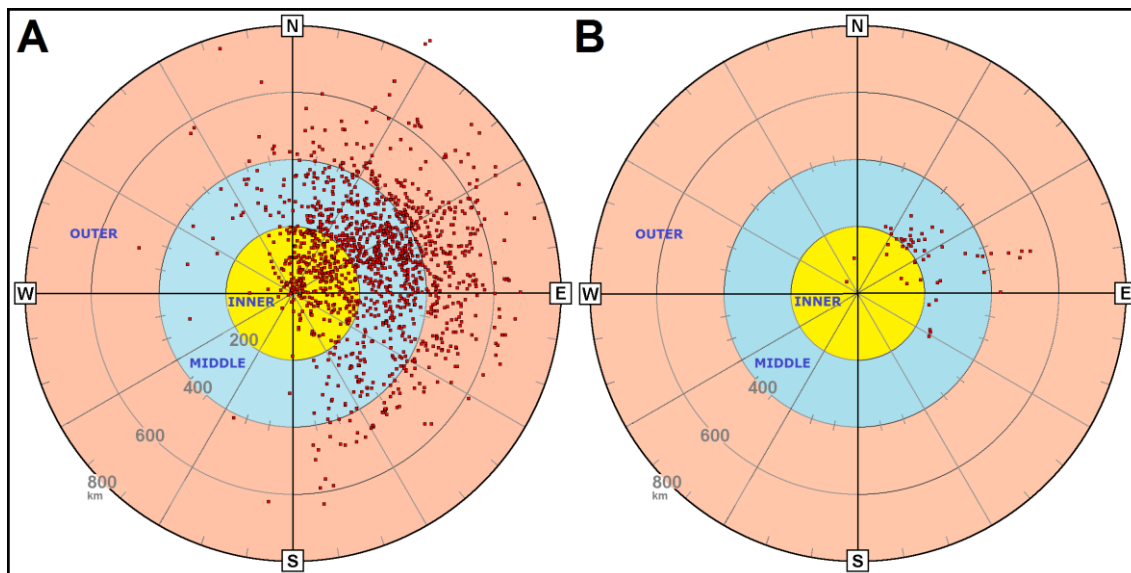
Figure 8: Polar plot of tornadogenesis positions (red dots) with respect to true-north-relative azimuth and range (km) from center for a) TCTOR, 1995–2017), b) Harvey. Inner, middle and outer annuli follow Edwards and Thompson (2014) convention for general radial-distance classification in tornadic TCs.
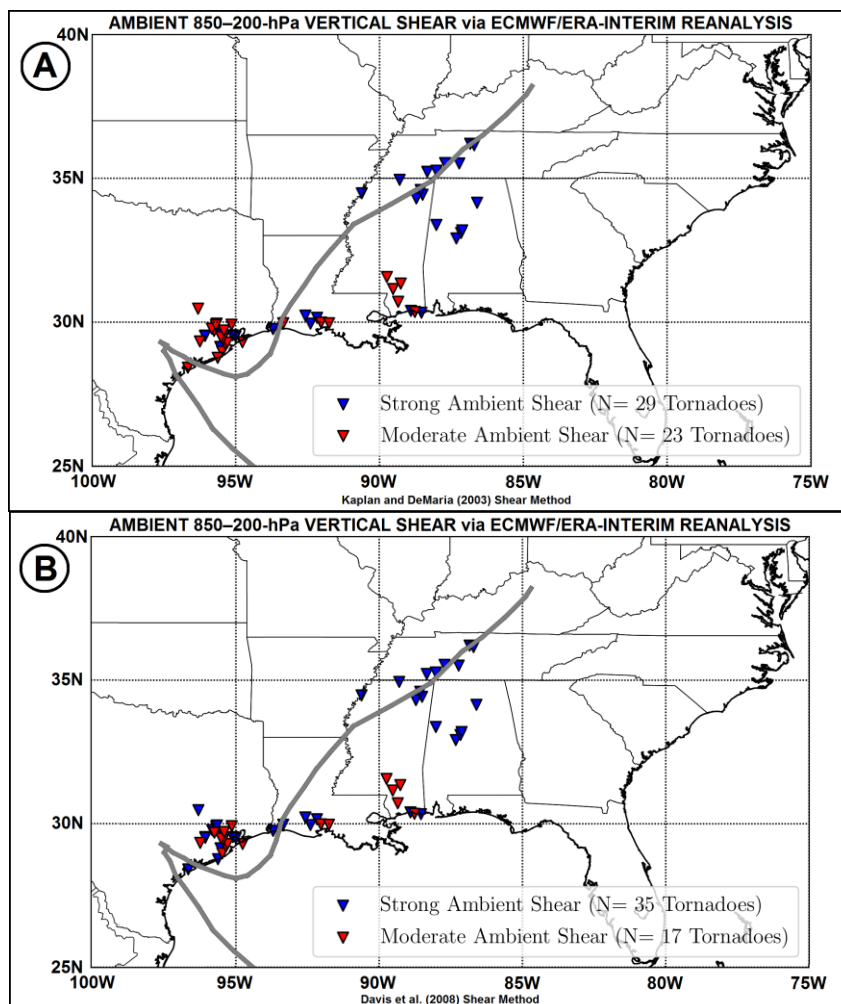
Figure 9: Tornadoes (triangles) colored by 850–200-hPa vertical-shear-vector magnitude at tornado time, averaged from r = 200–800 km from center position: moderate (red, 5–10 m s^{-1}) and strong (≥10 m s^{-1}). [None occurred under "weak" shear conditions.] Some proximal events may obscure each other. Thick gray line is the path of Harvey's center. Two methods are used: a) Kaplan and DeMaria (2003), employed by the SHIPS model, and b) Davis et al. (2008), extracting irrotational and nondivergent components within 500 km of center. Plots prepared by B. Schenkel.

only with TC intensity evolution (e.g., DeMaria 1996), but inland tornado potential in tropical cyclones (e.g., McCaul 1991; Verbout et al. 2007).

One common measure in the realm of TC analysis, modeling and prediction is the 850–200-hPa vertical-shear vector magnitude (Kaplan and DeMaria 2003), a crucial component of the Statistical Hurricane Intensity Prediction Scheme (SHIPS; DeMaria and Kaplan 1994). Systems with weak deep shear tend to reside in the tropical easterlies, while at higher latitudes, the rest come under the influence of prevailing midlatitude flows, as was apparent with Harvey. As analyzed via the ECMWF ERA-Interim Reanalysis (Dee et al. 2011), tornadoes with Harvey generally occurred under stronger ambient deep shear with time, and with northward and inland extent (Fig. 9). Only minor differences are apparent in ambient shear during tornado hour for two computational methods:

- Kaplan and DeMaria (2003), the SHIPS technique that includes the influence of the TC (Fig. 9a), and
- Davis et al. (2008), which effectively removes the TC from the kinematic field, by extracting the nondivergent and irrotational vector components from total wind at all grid points within 500 km of TC center (Fig. 9b).

From 925 hPa to the surface, a remnant low-level frontal zone lay across the Texas and Louisiana Coastal Plain on 25 August, moving northward (inland) and becoming diffuse above the surface through the 27th, but lingering at the surface and near the Louisiana coast through the 29th. A separate low-level cold front, related to the middle/upper-tropospheric, northern-stream, Great Lakes perturbation, moved southeastward across the central and southern Plains states to the Texas Gulf Coast on 27–30 August. Harvey merged with the front while moving inland for the final time over southwestern Louisiana, and that part of the baroclinic zone to its east became essentially indistinguishable from the older, pre-existing one. The combined boundary east of Harvey's center moved northward as a warm front across Mississippi, Alabama, and parts of western and middle Tennessee on 30–31 August. The associated maritime-tropical warm sector thermodynamically supported the tornado threat across the Mid-South and Tennessee Valley regions on the last two days of the tornadic episode.

On the mesoscale, satellite and radar-composite imagery (not shown) revealed a persistent area of clouds, precipitation and embedded deep convection inland through most of Harvey's Texas phase. Precipitation into and near the aforementioned remnant frontal zone kept the low-level air mass relatively stable farther inland. Only a narrow corridor within ≈50–80 mi (80-129 km) of the coastline and northeast through east of center destabilized sufficiently to support more than very brief, isolated tornado potential. Although observed soundings are absent over southeast Texas, a time series of surface-modulated Rapid Refresh model soundings (not shown), derived from the SPC environmental mesoanalysis archive (Bothwell et al. 2002; Dean et

al. 2006) and created for the SPC tornadic storm and environment database (Smith et al. 2014) project, indicated that the related cooling limited the surface-based inflow. Most of Harvey's nighttime tornadoes (0000-1159 UTC in Table 1) occurred in southeast Texas and near-coastal areas of Louisiana and Mississippi. In the shear-favored sector, within and south of the precipitation-modulated warm-frontal zone and near the coast, less nocturnal stabilization would be expected, and less occurred based on those model soundings and available Lake Charles, LA soundings (not shown).
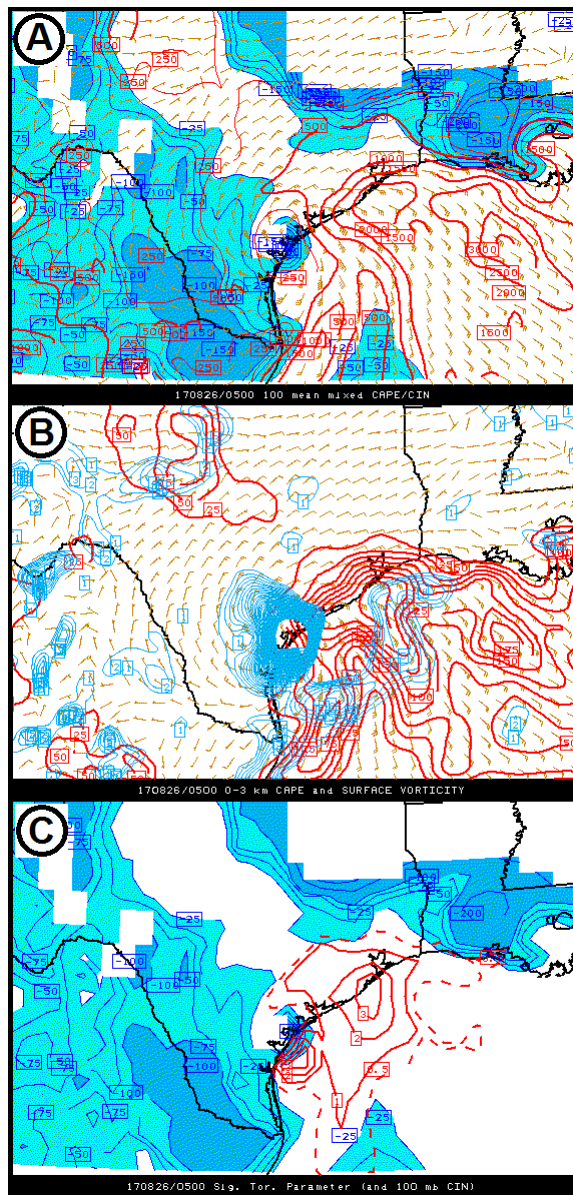

Figure 10: SPC mesoanalysis fields at 0500 UTC 26 August 2017: a) lowest-100-hPa mean mixed-layer CAPE in red, convective inhibition (MLCINH, blue shading) and surface winds (tan, full barb is 10 kt or 5 m s^{-1}); b) 0–3-km AGL CAPE (red) and surface vorticity (blue); and c) significant tornado parameter (red), with CINH.

Planar fields of the mesoanalysis data (e.g., Fig. 10) manifest the resulting mesoscale baroclinic zone

as a gradient in CAPE and convective inhibition (CINH). Low-level storm-relative helicity (SRH, not shown) strengthened northward through the same gradient with the increasingly backed surface flow, also overlapping with favorably low lifting condensation level, and weak but sufficient 0–6-km AGL bulk wind difference, to yield favorable values of, and a northward gradient in, the significant tornado parameter (Thompson et al. 2003). Temporal clusters of tornadoes (defined for our purposes as ≥3 within ±2 h of a given whole-hour UTC time) occurred within the baroclinic gradients throughout the 7-day tornadic phase. In the Texas portion, clusters also happened near surface thermal axes extending into gradients from the warm sector (e.g., Fig. 11).

4. FORECASTS and OPERATIONS

The forecast process for TCs as a whole is initiated and sustained by NHC until a system dissipates, loses tropical characteristics, or is passed to the Weather Prediction Center during a U.S. inland-decay stage. SPC coordinates with NHC and affected NWS offices via scheduled video hotline calls, regarding the tornado-threat wording employed in NHC's TC-forecast advisories. Here we focus specifically on the forecasts of the tornado hazard in the TC, which begin with SPC convective outlooks and continue through SPC mesoscale discussions and watches. In addition, NWS forecast-office warnings and follow-up severe-weather statements are issued for individual, localized tornado threats on the scale of cell motion.

a. SPC forecasts for Harvey

In general, outlooks cover convective-day (1200 to 1159 UTC) periods from 8 calendar days out to same day, are presented both in probabilistic and categorical form with technical discussion, and are driven by probabilistic forecasts of severe-storm event potential on an 80-km grid (or roughly within 25-mi radius of a given point within). For TC purposes, even though no specific hazard is specified graphically by convention at ≥2 days out, outlooks for TCs implicitly are intended for tornadoes. Their spatial extent is based off the NHC track and wind forecasts (with wind radii as proxy for storm size), as well as expected shear and instability characteristics, with room given for spatial and intensity uncertainty. As such, day-2 and day-3 outlooks *only for TCs can* be rendered to "slight" for 5%, in keeping with the day-1 tornado-only conversion convention. Beginning in 2018, general tornado probabilities were appended as a text table concluding day-2 outlooks. Day-2 specific-hazard graphics are planned; however, neither were done in 2017. Explicitly mapped tornado probabilities for Harvey began with the 0600 UTC day-1 outlook issuance, the first of five during that period. Otherwise, for a general overview of the suite of SPC forecast suite and more information on the timing and purpose of each set of forecasts in the SPC suite, see Edwards et al. (2015a).

Fig. 12 shows the suite of SPC outlooks valid for each day of Harvey's tornadic phase. Only one representative time issuance of day-2 and day-1 outlook graphics is shown for brevity; however, the full

suite of all archived outlook graphics and discussions for a given day of Harvey's impacts can be viewed via the date-based retrieval tool on the SPC outlooks website (https://www.spc.noaa.gov/products/outlook/). Please refer to those discussions for specifics on any given day's forecast reasoning. The very slow forecast and actual motion of Harvey ensured some outlook coverage for parts of southeast Texas on 6 of the 7 days. These areas were small and confined relatively close to the coast, where the boundary-layer air mass was expected to be at least marginally unstable, in an environment of enlarged hodographs (section 3). Outlook areas expanded considerably the last two days, commensurate with faster inland motion and enlarged areas of overland destabilization on those days. The outlooks were very consistent spatially on a given valid day, with only minor peripheral changes on meso-*β* and smaller scales. This can be expected with such slow TC motion and quite consistent NHC track and wind forecasts.

SPC issues mesoscale discussions (MDs), which have graphical and technical-text components. MDs appear on an unscheduled, as-needed basis, when conditions become favorable for overland tornadoes, to advise on the need for an upcoming watch (with watch-issuance probability), and to update conditions in existing watches. SPC issued 36 MDs for Harvey's tornado potential, beginning at 1519 UTC 25 August (not shown), before the first watch. The final MD was at 2323 UTC 1 September in the Carolinas, for a tornado watch along a peripheral warm front in which no tornadoes ultimately were confirmed. MD graphics highlighted salient mesoscale features within the broader circulation envelope, including those discussed in section 3 that confined and/or focused areas of greatest tornado potential. To obtain any individual SPC MD for Harvey, including specific discussion of forecast reasoning prior to and during each watch, please use the date-search tool on the MD website (https://www.spc.noaa.gov/products/md/).

In TCs, SPC issues as-needed tornado watches in consultation with affected (and sometimes nearby) local NWS forecast offices. Watches are county-based, though a legacy "watch box" polygon still is provided for aviation purposes. SPC updates threat areas within a watch hourly via status reports outlining counties still at risk, as well as irregular, unscheduled MDs in a meteorological sense (discussed above). Local NWS offices are responsible for clearing or extending counties in an existing watch. SPC watches may be issued adjacent to, or in replacement of, an existing watch as the threat shifts with the TC. In general, and especially in slow-moving, gradually evolving TCs like Harvey, tornado watches are valid for longer periods of time than the typical 6–9 h; Harvey's generally lasted 10–13 h. When meteorologically justifiable, the collaborative issuance of fewer and more widely temporally spaced tornado watches helps slightly to alleviate local NWS workload, in an already heavily strained TC situation loaded with both routine forecasts and atypical products, including: flooding and rainfall forecasts, hurricane local statements, marine products, emergency-management and media consultations, and many other time-consuming but necessary provisions of decision-support services via every
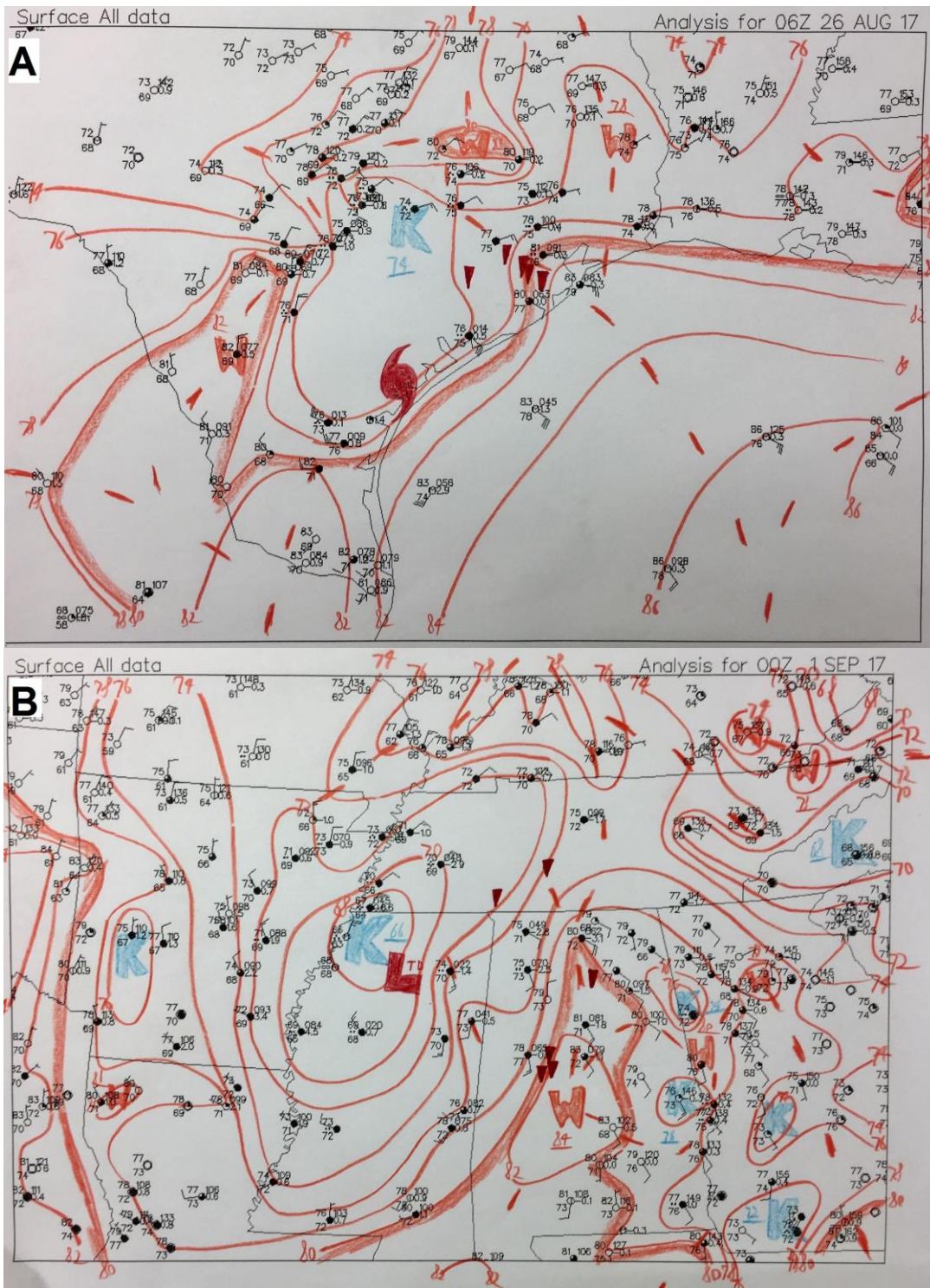
Figure 11: Meso-*α*-scale surface charts using conventional station plots (wind barbs in kt with full barbs 10 kt or 5 m s^{-1}, MSLP in hPa, thermodynamic variables in °F), with subjective hand analyses of surface temperature every 2 °F and the 80 °F isotherms highlighted, and conventional symbology. Charts valid: a) 0600 UTC 26 August 2017 and b) 0000 UTC 1 September 2017. Tornado locations ±2 h from analysis time are dark red triangles.
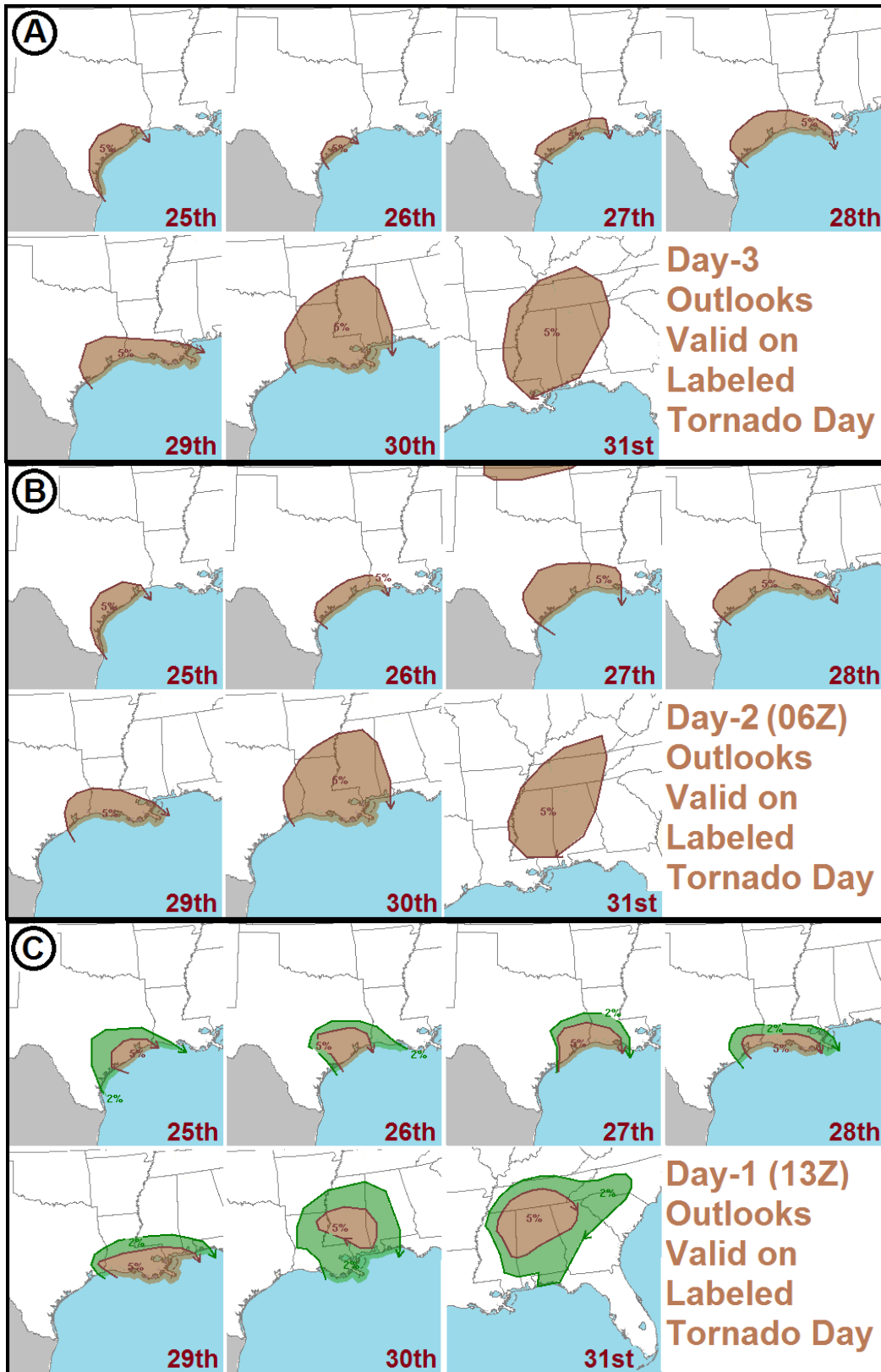
Figure 12: SPC probabilistic convective outlooks valid over the region affected by Harvey, for 24 h starting 1200 UTC on the labeled date: a) total-severe outlooks issued at 0730 UTC, 3 days in advance; b) total-severe outlooks issued by 0600 UTC, 2 days in advance; and c) day-1 outlooks issued by 1300 UTC the same day.
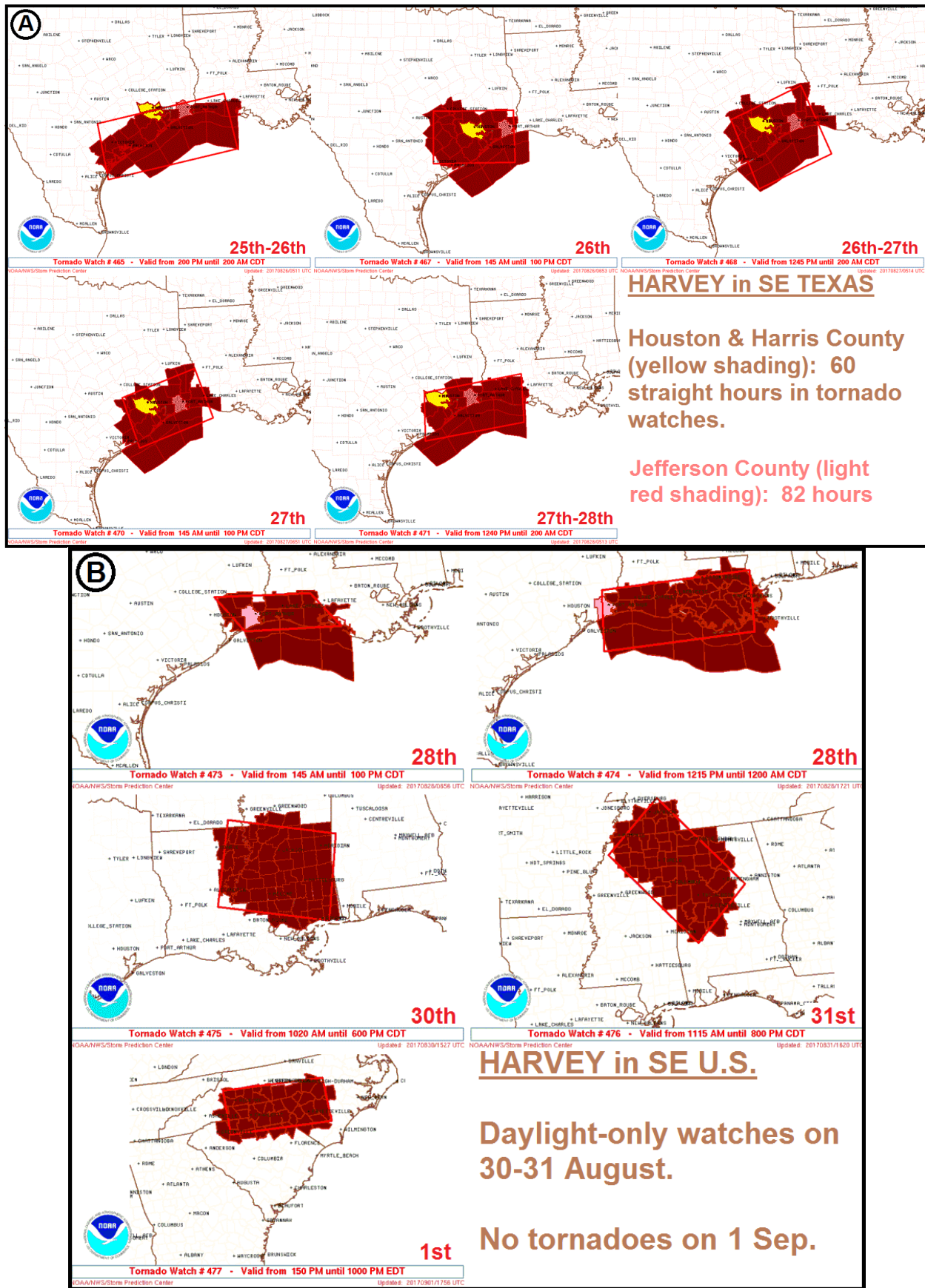
Figure 13: Tornado watches depicted by legacy polygon (bright red) and initial county configuration (dark red) with notes in lower-right panel, issued on: a) 25–27 August for southeast Texas and southwestern Louisiana, with Harris and Jefferson Counties, TX highlighted in yellow and light red, respectively; b) Southeastern U.S. for remainder of Harvey's inland lifespan.

14

available communications medium.

SPC watches for Harvey are illustrated in Fig. 13, and the entire text and graphical package for each one may be retrieved for more detailed scrutiny via date-archive search on the SPC watch website (https://www.spc.noaa.gov/products/watch/). Of particular interest is the amount of time the Houston Metro area, as exemplified by Harris County (yellow in Fig. 13) spent in tornado watches: 60 h continuously. A search of watches issued by SPC and its Kansas City, MO, predecessor, the National Severe Storms Forecast Center, reveals no other county containing a major city has been in continuous tornado watches for that long. In 2017, Houston was the fourth most-populous city in the U.S., and anchored the fifth most-populous metropolitan statistical area, from Census Bureau estimates. Based on available SPC archive data and meteorological histories, we believe no other major U.S. city or metro area has been under continuous tornado risk for a longer period of time than Harvey imposed on Houston. Parts of extreme southeast Texas in and near the Port Arthur were in tornado watches for 82 straight hours. No tornadoes are recorded in Harvey's remains for the 1 September convective day, during which the final tornado watch for Harvey was issued in the Carolinas.

b. Local forecast challenges

The long-duration tornado threat Harvey presented in southeast Texas meant dedicating a forecaster to tornado warnings for long stretches of time. At NWS Houston-Galveston (HGX), amidst the record flooding and required routine products, forecasters faced warning fatigue of their own, requiring at least a minimal rotation of forecasters in duties for continued warning operations. These circumstances compounded the challenge inherent to warning for TC tornadoes related to their rapid development, small size, and weak, transient radar signatures. Prior studies of TC tornadic radar signatures (e.g., Spratt et al. 1997; McCaul et al. 2004; Schneider and Sharp 2007; Martinaitis 2017) have developed a framework to aid forecasters in the tornado-warning decision. While this guidance helped forecasters during warning operations for Harvey, multiple tornadic storms had radar signatures well below guidance, while some nontornadic storms showed better-defined signatures. This will be further motivation for studying Harvey's tornadic and tornado-warned convection to understand better why some convection produced tornadoes and some did not (e.g., Nowotarski et al. 2018).

TC messaging presents a unique challenge for local NWS offices, because all four main hazards (storm surge inundation, wind, inland flooding and tornadoes) may impact the area simultaneously. HGX briefed all four hazards to local and state partners, but the inland flood threat received the most attention due to the possibility of long-lasting, catastrophic impacts. However, as Harvey approached southeast Texas, the increasing tornado threat warranted special attention, since local and state partners were increasing operations and resources in preparation for the flooding. The greatest local challenge came as the first major

rainband approached the HGX area, causing widespread flooding with a tornado threat. Figure 14 graphically summarizes three days of warnings from HGX. HGX issued 157 tornado warnings total: 154 from 1200 UTC 25 August 2017 to 1200 UTC 28 August 2017, then only three on the 29th. During the same 25–28 August time frame, HGX also issued 51 flash flood warnings, with a total of 62 for the event, while its forecast staff worked 6 straight days of 12-h shifts. At times on the night of 26–27 August, tornado and flash flood warnings overlapped to an overwhelming extent. Conflicting action statements from flash flood warnings (seek higher ground) and tornado warnings (seek shelter in lowest floor of a building which could be inundated from flooding) further confused the situation for people responding to the hazards.
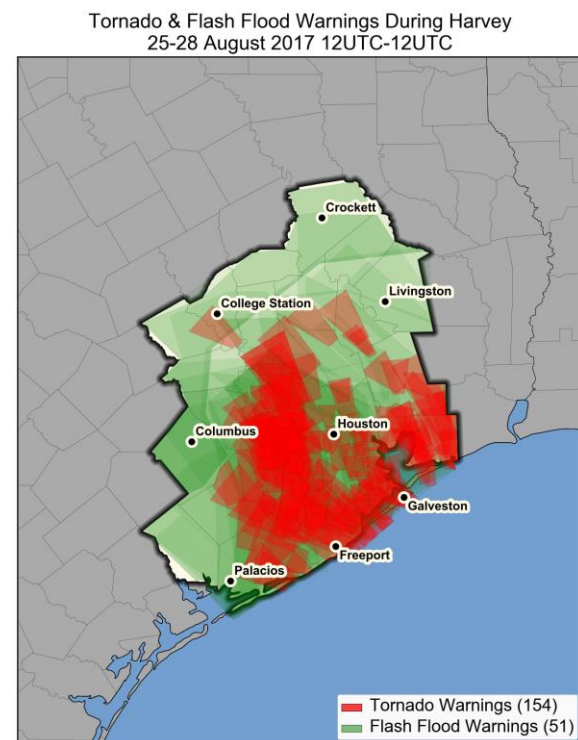

Figure 14: Tornado (red) overlying flash flood (green) warnings issued during the period 1200 UTC 25 August 2017 to 1200 UTC 27 August 2017 for the HGX county warning area (black outline). Deeper shading indicates more of each warning type in a given locale. Map prepared by P. Marsh.

5. SUMMARY and ADDITIONAL WORK

Hurricane Harvey and its inland-decay remnants spawned 52 tornadoes in a weeklong episode, from the Texas Coastal Plain across the Mississippi Delta region to the Mid-South (Figs. 3,9). The first 4 days featured not only a dense cumulative concentration of tornadoes within a relatively small part of southeast Texas, in and near the Houston metro area, but extreme, record rainfall. This yielded simultaneous inland hazards for tens of hours, day and night. No mesoscale region is known to have been under a continuous tornado risk longer than southeast Texas during Harvey, which included a large-city record 60 h of tornado watches in the Houston metropolitan area.

In terms of tornadic path characteristics, damage ratings, and spatial distribution with respect to TC center, Harvey conformed rather closely to TCTOR at large (section 2b). Its most outstanding characteristic was sheer persistence. Being otherwise well-behaved with respect to climatology, and with a relative concentration near surface baroclinic zones (section 3), Harvey's tornado production revealed few particularly strong anomalies, surprises or unusual characteristics on which to focus special meteorological attention, acknowledging the relative lull in the middle of its weeklong tornadic phase that is fairly straightforwardly attributable to lack of suitably unstable air inland.

Still, examination of Harvey's tornado production will have value and will continue. The realm of TC tornadoes in general has avenues of study yet to mature, with improvements still to be made in terms of forecasting and understanding with newer tools (e.g., discussions in E12 and Edwards and Picca 2016). Analyses such as that in Fig. 9 will be expanded to other TCs and relative-framework perspectives, in order to determine the relationship of ambient deep shear to TC-tornado density, distribution and damage. Environmental analyses (section 3) also will be expanded to present a fuller picture of Harvey's tornado environment, as well as for inclusion in multi-TC meteorological climatologies.

Harvey's TDSs are being included in the updated, enlarged and formalized version of the Edwards and Picca (2016) preliminary study. A companion study to this one in the same conference (Nowotarski et al. 2018) is examining the relationships between TDS appearances and storm environment for Harvey's Texas tornadic cells, and may be expanded to later phases of Harvey, as well as other TCs.

When holistically intertwined with Harvey's other hazards, and preparedness and messaging efforts in particular, the part of Harvey's tornadic phase affecting western Gulf Coastal Plain offers lessons for further work. One such avenue to pursue is warning- and emergency-preparedness efforts targeting a lesser yet still potentially deadly hazard (tornadoes) in the face of a greater and deadlier one (extensive flooding). That includes messaging the tornado threat in a warning and safety sense when the usual indoors advice (lowest level, smallest part, away from windows) may be underwater. Perhaps the most lasting positive effects of Harvey on the integrated warning system will be more sociological and preparedness-based than meteorological.

Bridging the gap between the watch/MD realm and warnings, and improving the quality and continuity of information flow in high-impact weather events, are among the goals of the Forecasting a Continuum of Environmental Threats (FACETs) effort (Rothfusz et al. 2018). FACETs involves provision of high-resolution, probabilistic hazard information, with social-science input aimed at most effectively communicating the threat to diverse audiences. TC tornadoes justifiably can be included in such efforts, being:

1) A subset of the nationwide annual tornado threat,
2) A hazard largely removed from the attention-commanding central core region of TCs (E12), and
3) The dominant proportion of late-summer tornado production in the U.S. climatologically (Edwards et al. 2012).

Harvey's unique duration and intensity of flood threat, overlapping with multiday tornado risk, offer an extreme yet useful multi-hazard example for potential analysis in the FACETs context.

ACKNOWLEDGMENTS

REFERENCES

Barbour, G. B., 1924: Waterspout and tornado within a typhoon area. *Mon. Wea. Rev.*, **52**, 106–107.

Blake, E. S., and D. A. Zelinsky, 2018: National Hurricane Center tropical cyclone report: Hurricane Harvey, 76 pp. [Available online at https://www.nhc.noaa.gov/data/tcr/AL092017_Harvey.pdf.]

Bothwell, P. D., J. A. Hart, and R. L. Thompson, 2002: An integrated three-dimensional objective analysis scheme in use at the Storm Prediction Center. Preprints, *21st Conf. on Severe Local Storms*, San Antonio, TX, Amer. Meteor. Soc., J117–J120.

Burgess, D. W., M. A. Magsig, J. Wurman, D. C. Dowell, and Y. P. Richardson, 2002: Radar observations of the 3 May 1999 Oklahoma City tornado. *Wea. Forecasting*, **17**, 456–471.

Curtis, L., 2004: Midlevel dry intrusions as a factor in tornado outbreaks associated with landfalling tropical cyclones from the Atlantic and Gulf of Mexico. *Wea. Forecasting*, **19**, 411–427.

Davis, C., C. Snyder, and A. C. Dislake Jr., 2008: A vortex-based perspective of eastern Pacific tropical cyclone formation. *Mon. Wea. Rev.*, **136**, 2461–2477.

Dean, A. R., R. S. Schneider, and J. T. Schaefer, 2006: Development of a comprehensive severe weather forecast verification system at the Storm Prediction Center. Preprints, 23nd Conf. on Severe Local Storms, Saint Louis MO, Amer. Meteor. Soc., P2.3.

Dee, D. P., and Coauthors, 2011: The ERA-Interim reanalysis: Configuration and performance of the data assimilation system. *Quart. J. Roy. Meteor. Soc.*, **137**, 553–597.

DeMaria, M., 1996: The effect of vertical shear on tropical cyclone intensity change. *J. Atmos. Sci.*, **53**, 2076–2087.

——, and J. Kaplan, 1994: A Statistical Hurricane Intensity Prediction Scheme (SHIPS) for the Atlantic basin. *Wea. Forecasting*, **9**, 209–220.

Edwards, R., 2010: Tropical cyclone tornado records for the modernized National Weather Service era. Preprints, *25th Conf. on Severe Local Storms*, Denver, CO, Amer. Meteor. Soc., P2.7.

——, 2012: Tropical cyclone tornadoes: A review of knowledge in research and prediction. *Electronic J. Severe Storms Meteor.*, **7** (6), 1–61.

——, and A. E. Pietrycha, 2006: Archetypes for surface baroclinic boundaries influencing tropical cyclone tornado occurrence. Preprints, *23rd Conf. on Severe Local Storms*, Saint Louis, MO, Amer. Meteor. Soc., P8.2.

——, and R. L. Thompson, 2014: Reversible CAPE in tropical cyclone tornado regimes. Proc., *27th Conf. on Severe Local Storms*, Madison, WI, Amer. Meteor. Soc., P88.

——, and J. C. Picca, 2016: Tornadic debris signatures in tropical cyclones. Proc., *28th Conf. on Severe Local Storms*, Portland, OR, Amer. Meteor. Soc., P162.

——, A. R. Dean, R. L. Thompson and B. T. Smith, 2012: Convective modes for significant severe thunderstorms in the contiguous United States. Part III: Tropical cyclone tornadoes. *Wea. Forecasting*, **27**, 1114–1135.

——, J. G. LaDue, J. T. Ferree, K. Scharfenberg, C. Maier, and W. L. Coulbourne, 2013: Tornado intensity estimation: Past, present, and future. *Bull. Amer. Meteor. Soc.*, **94**, 641–653.

——, G. W. Carbin, and S. F. Corfidi, 2015a: Overview of the Storm Prediction Center. Preprints, *13th History Symp.*, Phoenix, AZ, Amer, Meteor. Soc., 1.1.

——, B. T. Smith, R. L. Thompson and A. R. Dean, 2015b: Analyses of radar rotational velocities and environmental parameters for tornadic supercells in tropical cyclones. Proc., *37th Conf. on Radar Meteorology*, Norman, OK, Amer. Meteor. Soc., 5A.3.

Hales, J. E. Jr., 1988: Improving the watch/warning program through use of significant event data. Preprints, *15th Conf. on Severe Local Storms*, Baltimore, MD, Amer. Meteor. Soc., 165–168.

Hill, E. L., W. Malkin and W. A. Schulz Jr., 1966: Tornadoes associated with cyclones of tropical origin—practical features. *J. Appl. Meteor.*, **5**, 745–763.

Johns, R. H., and C. A. Doswell III, 1992: Severe local storms forecasting. *Wea. Forecasting*, **7**, 588–612.

Kaplan, J., and M. DeMaria, 2003: Large-scale characteristics of rapidly intensifying tropical cyclones in the North Atlantic basin. *Wea. Forecasting*, **18**, 1093–1108.

Martinaitis, S., 2017: Radar observations of tornado-warned convection associated with tropical cyclones over Florida. *Wea. Forecasting*, **32**, 165–185.

McCaul, E. W. Jr., 1987: Observations of the Hurricane "Danny" tornado outbreak of 16 August 1985. *Mon. Wea. Rev.*, **115**, 1206–1223.

——, 1991: Buoyancy and shear characteristics of hurricane-tornado environments. *Mon. Wea. Rev.*, **119**, 1954–1978.

——, D. E. Buechler, S. J. Goodman, and M. Cammarata, 2004: Doppler radar and lightning network observations of a severe outbreak of tropical cyclone tornadoes. *Mon. Wea. Rev.*, **132**, 1747–1763.

Moore, T. W., N. J. Sokol, and R. A. Blume, 2017: Spatial distributions of tropical cyclone tornadoes by intensity and size characteristics. *Atmosphere*, **8**, 1–13, doi: 10.3390/atmos809016.

Novlan, D. J., and W. M. Gray, 1974: Hurricane-spawned tornadoes. *Mon Wea Rev.*, **102**, 476–488.

Nowotarski, C. J., R. Cheatham, S. Overpeck, and R. Edwards, 2018: Comparison of tornadic and nontornadic convective cells in Hurricane Harvey. Proc., *29th Conf. on Severe Local Storms*, Stowe, VT, Amer. Meteor. Soc., 175.

Rappaport, E. N., 2014: Fatalities in the United States from Atlantic tropical cyclones: New data and interpretation. *Bull. Amer. Meteor. Soc.*, **95**, 341–346.

Ryzhkov, A. V., T. J. Schuur, D. W. Burgess, and D. S. Zrnić, 2005: Polarimetric tornado detection. *J. Appl. Meteor.*, **44**, 557–570.

Rothfusz, L. P., R. S. Schneider, D. Novak, K. E. Klockow-McClain, A. E. Gerard, C. D. Karstens, G. J. Stumpf, and T. M. Smith, 2018: FACETs: A proposed next-generation paradigm for high-impact weather forecasting. *Bull. Amer. Meteor. Soc.*, **99**, 2025−2043.

Schaefer, J. T., and R. Edwards, 1999: The SPC tornado/severe thunderstorm database. Preprints, *11th Conf. on Applied Climatology*, Dallas, TX, Amer. Meteor. Soc., 6.11.

Schneider, D., and S. Sharp, 2007: Radar signatures of tropical cyclone tornadoes in central North Carolina. *Wea. Forecasting*, **22**, 278–286.

Smith, B. T., R. L. Thompson, and A. R. Dean, 2014: The Storm Prediction Center tornadic storm and environment database: Development and application. Proc., *27th Conf. on Severe Local Storms*, Nashville, TN, Amer. Meteor. Soc., 17.1.

——, ——, ——, and P. T. Marsh, 2015: Diagnosing the conditional probability of tornado damage rating using environmental and radar attributes. *Wea. Forecasting*, **30**, 914–932.

Snellman, L. W., 1982: Impact of AFOS on operational forecasting. Preprints, *9th Conf. on Weather Forecasting and Analysis*, Seattle, WA, Amer. Meteor. Soc., 13–16.

Spratt, S. M., D. W. Sharp, P. Welsh, A. C. Sandrik, F. Alsheimer, and C. Paxton, 1997: A WSR-88D assessment of tropical cyclone outer rainband tornadoes. *Wea. Forecasting*, **12**, 479–501.

Thompson, R. L., and M. D. Vescio, 1998. The destruction potential index—A method for comparing tornado days. Preprints, *19th Conf. on Severe Local Storms*, Minneapolis, MN, Amer. Meteor. Soc., 280–282.

——, R. Edwards, J. A. Hart, K. L. Elmore, and P. Markowski, 2003: Close proximity soundings within supercell environments obtained from the Rapid Update Cycle. *Wea. Forecasting*, **18**, 1243–1261.

Verbout, S. M., D. M. Schultz, L. M. Leslie, H. E. Brooks, D. J. Karoly and K. L. Elmore, 2007: Tornado outbreaks associated with landfalling hurricanes in the North Atlantic Basin: 1954–2004. *Meteor. Atmos. Phys.*, **97**, 255–271.

Zhang, J., 2015: Multi-Radar Multi-Sensor (MRMS) quantitative precipitation estimation (QPE), 10 pp. [Available online at https://www.nssl.noaa.gov/about/events/review2015/science/files/Zhang_NSSLReview2015_MRMS-Hydro.pdf.]